J Mater Sci (2015) 50:4095–4103
DOI 10.1007/s10853-015-8965-5

Microfibrillated cellulose-SiO_2 composite nanopapers produced by spray deposition

Lisiê Ferreira Krol[1,2] · Davide Beneventi[1,4,5] · Fannie Alloin[2,3] · Didier Chaussy[1,4,5]

Received: 19 December 2014 / Accepted: 10 March 2015 / Published online: 19 March 2015

Abstract Microfibrillated cellulose (MFC)-SiO_2 nanopapers were prepared using a rapid spray deposition technique. Large area ($\sim$310 cm^2) composite nanopapers with thickness and SiO_2 content varying from 16 to 92 μm and 0 to 33 %, respectively, were prepared in less than 30 min with nearly complete nanoparticle retention in the cellulose mat. In the presence of an excess of MFC, SiO_2 nanoparticles formed large clusters embedded in a dense and continuous cellulose matrix which conferred to the composite an extremely low permeability to air, i.e., below 2 nm^2. For silica mass fraction above 20 %, SiO_2 clusters induced a net increase in air permeability and ionic conductivity up to 12 nm^2 and 1.5 mS cm^{-1} for a SiO_2 content of 33 %. Despite the addition of an inert phase, composite nanopapers displayed mechanical properties, viz. Young's modulus and internal cohesion higher than 2.2 GPa and 913 J m^{-2}, outperforming those of most conventional papers. This study demonstrates that MFC-SiO_2 nanopapers fabricated by spray deposition can be an alternative to PE/PP membranes as separators in Li-ion batteries and, in general, that spray deposition is a promising method for the rapid fabrication of large area composite nanopapers.

✉ Davide Beneventi
davide.beneventi@pagora.grenoble-inp.fr

Lisiê Ferreira Krol
lisiekrol@gmail.com

Fannie Alloin
fannie.alloin@grenoble-inp.fr

Didier Chaussy
didier.chaussy@pagora.grenoble-inp.fr

1 Univ. Grenoble Alpes, LGP2, 38000 Grenoble, France

2 CNRS, LEPMI, 38000 Grenoble, France

3 Univ. Grenoble Alpes, LEPMI, 38000 Grenoble, France

4 CNRS, LGP2, 38000 Grenoble, France

5 Agefpi, LGP2, 38000 Grenoble, France

Introduction

Recent progress in microfibrillated cellulose (MFC) production led to a neat drop in energy consumption [1, 2], and to the upscale of the MFC fabrication process from laboratory grinders/microfluidizers to semi-industrial pilot plants [3]. Even if a full commercial scale production of MFC has not been achieved yet, the availability of large amounts of cellulose nanofibres promoted the development of new materials using MFC as the main component and of the associated production processes. Leaving aside thermoplastic polymer nanocomposites [4, 5], where MFC, used as reinforcing phase, represents a small fraction of the composite mass, today MFC is mostly used as a building block in the elaboration of bulk or composite nanopaper for both high strength/barrier packaging [6, 7], and energy/electronic applications [8, 9].

Several procedures, based on filtration dewatering of diluted MFC suspensions [10–12], have been proposed to produce MFC nanopaper with excellent mechanical and barrier properties. Nevertheless, an excessive sheet fabrication time, exceeding 60 min, represents a bottleneck for process scale-up. Fairly recent works [13–15] demonstrated that this limitation can be surpassed by processing high consistency (i.e., 0.6–2 %) MFC suspensions and that single component and composite nanopaper can be fabricated in less than 10–15 min, thus paving the way to the upscale of nanopaper production on continuous paper machines [16].

Owing to the outstanding mechanical properties of cellulose nanofibers [17] and the progress in their production

and processing as large area nanopaper sheets, MFC is being considered for use in the fabrication of functional nanopaper for electric/energy storage applications.

When blended with copper [18], graphite [19] or polypyrrole [20] microparticles at weight fractions ranging between 3 and 10 %, MFC generates a nanofibre network surrounding the conducting particles which leads to the formation of high conductivity and flexible composite nanopapers. The use of electrochemically active materials as functional phase, i.e., graphite [16, 19], or $LiFePO_4$ [21], allows processing flexible electrodes for Li-ion batteries. On the other hand, inert alumina microparticles [22] or silica nanoparticles [23, 24], effectively prevent the dense packing of cellulose nanofibers favouring the formation of nanoporous papers with controlled porosity and excellent performances as separators in Li-ion batteries. The full potential of functional nanopaper formulation and processing has been recently demonstrated by Leijonmarck et al. [25] who integrated a complete device, i.e., a Li-ion cell, in a single nanopaper sheet by the sequential filtration of MFC dispersions containing the battery components.

Despite interesting performances, composite nanopaper fabrication via the filtration of nanoparticle aqueous suspensions remains a slow process (1–24 h filtration) which is not viable for a full-scale production of large area electrodes/complete cells. Thereafter, the aim of this work was to mimic unit operations present in industrial paper machines and to demonstrate that spray deposition to a moving blotter (used as filtration medium) [14–16], followed by the transfer of the blotter-supported film to the vacuum-dewatering and the drying sections and the final film peel off, can be a viable method for the full-scale production of MFC-SiO_2 composite nanopaper separators.

Experimental

Materials

MFC was produced at FCBA (Grenoble) using a commercial bleached hardwood (birch) kraft pulp (UPM Betula). MFC was prepared according to a mechano-enzymatic protocol followed by homogenization at high pressure [1], and supplied in the form of a 2 % consistency hydrogel. Silicon dioxide nanopowder with primary particle size of 5–15 nm diameter, and nominal particle and bulk densities of 2400 ± 200 and 68 kg m^{-3}, respectively, was supplied by Sigma-Aldrich.

MFC-SiO_2 sheets preparation

MFC-SiO_2 slurries with silica weight fractions (on dry solids) ranging between 11 and 33 % were prepared by adding 5 up to 20 g of SiO_2 to 2 kg the MFC hydrogel under gentle stirring. After the complete wetting of silica nanopowder, slurries were intensively stirred using a high-speed kitchen mixer. For all tested conditions, MFC-SiO_2 slurries had nearly constant pH and electrical conductivity, i.e., 7 ± 1 and 400 ± 50 μS cm^{-1}, respectively.

Composite sheets were prepared by spray deposition of MFC-silica slurries on a 25 cm diameter wet coated cardboard (which acted as smooth filter) using an in-house assembled spray coater [10, 15]. As schematized in Fig. 1, the coater was composed by a variable speed conveyor and a commercial high-pressure spray system (paint crew, Wagner) which were operated at a speed ranging from 1 to 4 m min^{-1} and at a constant slurry mass flow of 0.75 kg min^{-1}, respectively.

The excess water was removed from the deposited slurry by vacuum suction using the sheet forming section of a rapid köthen hand sheet former (Fig. 1e). After dewatering, a coated cardboard was superposed to the wet MFC-SiO_2 mat, and the whole stack was compressed using a 3 kg roll (Fig. 1f). The wet mat sandwiched between the two cardboards was then dried in the vacuum drying section of the rapid köthen hand sheet former during 20 min at 90 °C (Fig. 1g). Finally, the two cardboards were gently peeled off, and a 20 cm diameter, self-standing, MFC-SiO_2 composite film was obtained (Fig. 1h).

Under the assumption of complete MFC and SiO_2 retention on the wet cardboard during the fabrication process and their homogeneous distribution over the main impact zone, the basis weight (bw_{MFC}) of the MFC film was calculated from the spray operating conditions and the geometry of the experimental set up using the Eq. [15].

$$bw_{MFC} = \frac{\dot{m} \cdot c}{2D \cdot \tan\theta \cdot V}, \quad (1)$$

where $\dot{m}$ and c are the mass flow and the consistency of the MFC-SiO_2 slurry, respectively, D is the distance of the spray nozzle from the substrate (0.36 m), V is the conveyor speed and θ is the spray jet angle (i.e., 56°). Basis weights obtained from Eq. (1) and experimental ones were used to evaluate the retention of MFC and SiO_2 in the composite sheet.

MFC-SiO_2 sheets characterization

In order to assess MFC and SiO_2 distribution, the surface and the cross section of composite films were imaged by electronic microscopy (SEM-FEG, Zeiss Ultra 55).

The overall film thickness was measured with a mechanical caliper (Adamel Lhomargy, MI20) and used to calculate the film (apparent) geometric density, ρ^{i}_{App}, from the corresponding basis weight. The film (apparent) gravimetric density, ρ^{ii}_{App}, was also determined using a

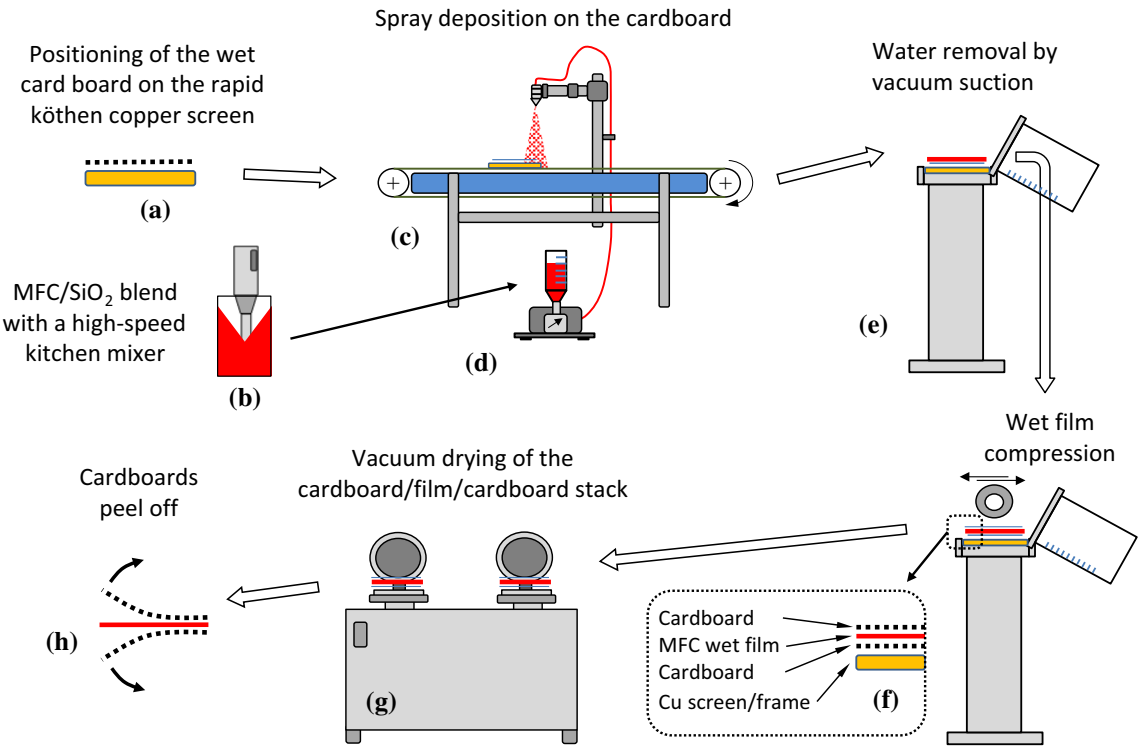

Fig. 1 Scheme of MFC-SiO_2 composite nanopaper fabrication process. **a** Positioning of the wet cardboard on the rapid köthen copper screen, **b** pre-mixing of MFC and SiO_2 nanopowder, **c** variable speed conveyor, **d** high-pressure pump feeding the spray nozzle, **e** dewatering section of the rapid köthen handsheet former, **f** cardboard stacking and compression, **g** vacuum drying in the drying section of the rapid köthen handsheet former, **h** removal of the two cardboards and final composite sheet

Mettler-Toledo measurement kit, water and propanol as test liquids and the equation.

$$\rho^{ii}_{\mathrm{App}} = \frac{m_a}{m_a - m_l} \cdot (\rho_l - \rho_a) + \rho_a, \tag{2}$$

where m_a, m_l are the sample weights in air and in the test liquid, and ρ_a and ρ_l are the densities of air and of the test liquid, respectively.

The geometric and gravimetric apparent densities and the nominal SiO_2 weight fraction were used to calculate air (ϕ_{Air}), SiO_2 ($\phi_{\mathrm{SiO_2}}$) and MFC volume fractions (ϕ_{MFC}) according to the Eq. [18]:

$$\phi_{\mathrm{Air}} \cong W_{\mathrm{SiO_2}}\left(1 - \frac{\rho_{\mathrm{App}}}{\rho_{\mathrm{SiO_2}}}\right) + W_{\mathrm{MFC}}\left(1 - \frac{\rho_{\mathrm{App}}}{\rho_{\mathrm{Cell}}}\right), \tag{3}$$

$$\phi_{\mathrm{SiO_2}} = W_{\mathrm{SiO_2}}\frac{\rho_{\mathrm{App}}}{\rho_{\mathrm{SiO_2}}}, \tag{4}$$

$$\phi_{\mathrm{MFC}} = W_{\mathrm{MFC}}\frac{\rho_{\mathrm{App}}}{\rho_{\mathrm{Cell}}}, \tag{5}$$

where ρ_{App} is the film apparent density, $\rho_{\mathrm{SiO_2}}$ and ρ_{Cell} are the silica particle and cellulose densities (i.e., 2400 and 1500 kg m^{-3}, respectively) and $W_{\mathrm{SiO_2}}$ and W_{MFC} are silica and MFC weight fractions in the film. According to the different determination principle, the difference between air volume fractions obtained by the geometric and the gravimetric method was used to evaluate the sheet open porosity.

The film intrinsic air permeability was measured using a Bendtsen tester (Lorentzen and Wettre) operated with a differential pressure of 19.2 kPa, and it was expressed using the Darcy's formalism, namely

$$k = \frac{Q \cdot \mu \cdot d}{S \cdot \Delta P}, \tag{6}$$

where Q is the air flow passing through the composite film, S is the cross sectional area of the test sample (i.e., 10 cm^2), μ is air dynamic viscosity, d is the film thickness and ΔP is the applied pressure.

In order to measure the ionic conductivity of composite nanopapers when used as separators in Li-ion batteries, samples were cut in a 9 mm diameter discs, dried in a Buchi oven under vacuum (10^{-2} mbar) at 130 °C for 24 h and transferred in an Ar glove box. After impregnation with a liquid electrolyte of 0.01 M lithium hexafluorophosphate ($LiPF_6$) in ethylene carbonate (EC)/dimethyl carbonate (DMC) (1/1, m/m), the samples were assembled into Swagelok® cells, between two blocking electrodes and ionic conductivity was measured through electrochemical impedance spectroscopy (EIS) (HP 4192A). Measurements

were performed using a frequency range of 10 MHz–5 Hz, an applied voltage of 20 mV and the temperature was stabilized at 25 °C (Vötsch VTM 4004 climatic chamber). The electrochemical properties were provided as the average of at least five replicates and expressed as the ratio between the conductivity of the impregnated film (C) and of the electrolyte ($C_0 = 0.073$ mS cm^{-1} at 25 °C). In order to comply with the concentration of standard liquid electrolytes used in Li-ion batteries, additional conductivity measurements were performed using a 1 M $LiPF_6$ electrolyte. Owing to the good wetting properties of cellulose and SiO_2 by carbonated solvents [23] and the limited swelling of the MFC network, ionic conductivity measurements were also used (with air permeability) to estimate the pores connectivity in MFC-SiO_2 sheets.

Mechanical properties were evaluated by (i) traction tests (Instron, 5969) on 5 × 1.5 cm strips with a strain rate of 5 mm min^{-1} and (ii) internal bond strength (Scott Bond, IDM test IBT-10A) according to the Tappi T569 standard. Tests were performed after 24 h sample storage under controlled conditions, i.e., 50 % relative humidity and 23 °C and all properties are provided as the average of five replicates.

Results and discussion

Figure 2 shows that the use of the spray deposition technique allowed obtaining homogeneous MFC-SiO_2 sheets with basis weight ranging from 14 to 42-62 g m^{-2} when the conveyor speed was decreased from 4 to 1 m min^{-1}. The addition of SiO_2 and the corresponding increase of the slurry consistency from 2 to 3 % led to an increase of both basis weight (Fig. 2a) and film opacity (Fig. 2b). The good agreement between experimental data and basis weight calculated using Eq. (1) was interpreted as reflecting the good processability of MFC-SiO_2 slurries, which were homogeneously distributed over the cardboard, and the almost complete retention of both MFC and SiO_2 particles in the composite sheet during the dewatering stage.

Under the tested conditions, i.e., pH 7 ± 1 and conductivity 400 ± 50 µS cm^{-1}, both cellulose [26, 27], and silica nanoparticles [28, 29], are negatively charged. Thereafter, in the presence of moderate conductivity, the electrolyte concentration is not sufficient to screen surface charges, and repulsive double-layer forces prevent the adhesion between cellulose and silica surfaces [28, 30]. Due to the absence of flocculation between MFC and silica, the high retention of cellulose nanofibres and of the SiO_2 nanopowder was associated to the formation of a dense MFC network which was supposed to prevent both nanofibre and SiO_2 to flow out of the hydrogel during filtration [10, 14–16].

SEM analysis shows that, in the absence of SiO_2 (Fig. 3a–c), MFC formed a dense film with no visible defects. The film surface presented irregular spots which were ascribed to the slight surface damage during film manufacturing (i.e., cardboard peel off). This defect was visible also in the presence of SiO_2.

The addition of SiO_2 and the progressive increase of its mass fraction led to the formation of large SiO_2 nanoparticle clusters embedded in a continuous MFC matrix (Fig. 3). SEM images show that for a SiO_2 mass fraction up to 20 %, the composite sheets display a stratified structure with no detectable mixture between the two phases at the particle scale. MFC forms a bulky matrix and SiO_2 large

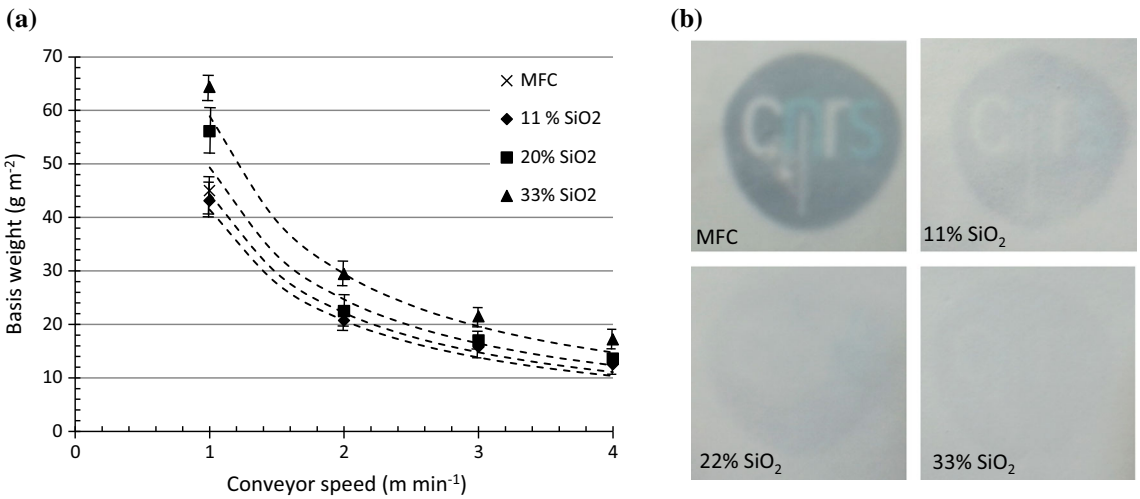

Fig. 2 Production of MFC-SiO_2 films by spray deposition. **a** Basis weight of the composite films plotted as a function of the conveyor speed and SiO_2 weight fraction [*dotted lines* represent basis weights calculated using Eq. (1)]. **b** Images of sheets obtained at a conveyor speed of 1 m min^{-1} and increasing SiO_2 weight fractions

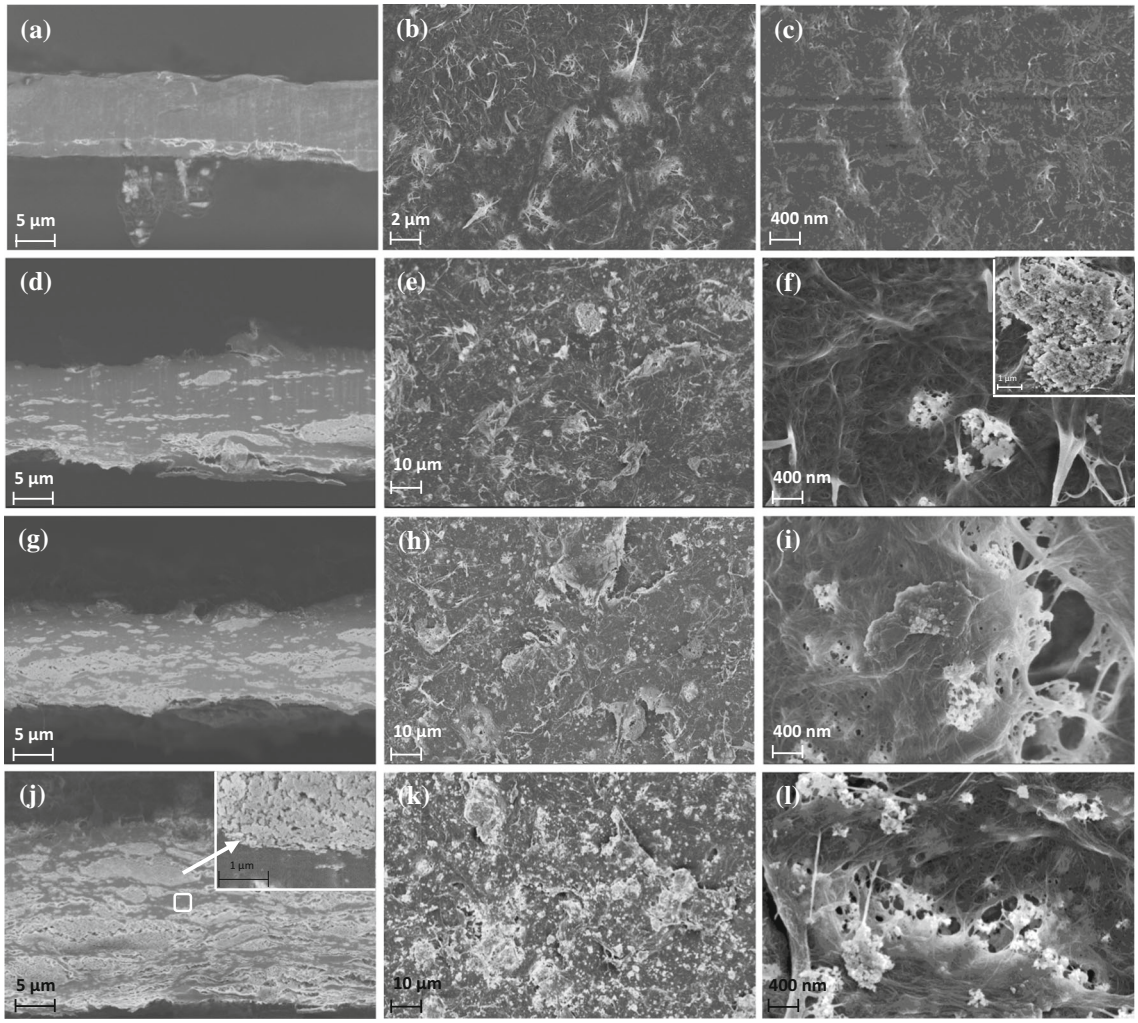

Fig. 3 SEM images of MFC-SiO_2 composites. MFC sheet, **a** cross section at ×2000 and surface at (**b**) ×5000 and (**c**) ×20000 magnification. 11 % SiO_2 sheet, **d** cross section at ×2000 and surface at (**e**) ×1000 and (**f**) ×20000 magnification. 20 % SiO_2 sheet, **g** cross section at ×2000 and surface at (**h**) ×1000 and (**i**) ×20000 magnification. 33 % SiO_2 sheet sheets, **j** cross section at ×2000 and surface at (**k**) ×1000 and (**l**) ×20000 magnification

macroporous clusters. The further increase of silica mass fraction destructured the MFC matrix and percolation paths formed among SiO_2 (Fig. 3i–j). For all tested conditions, MFC was not detected inside silica clusters (insets in Fig. 3) leading to the assumption of an incomplete dispersion of SiO_2 in the hydrogel.

This behaviour was ascribed to nanoparticles irreversible agglomeration during synthesis and drying, the subsequent incomplete dispersion of the SiO_2 nanopowder in water and the formation of large aggregates which, for the commercial silica used in this study, have an average size of 740 nm [29].

As illustrated by SEM images and by the plot of the sheet basis weight versus thickness (Fig. 4), silica induced a general increase in the film thickness and the apparent geometric density, provided by the slope of interpolating straight lines in Fig. 4, dropped from 1440 to 730 kg m^{-3} when considering bulk MFC and films containing 33 % of SiO_2, respectively. The apparent sheet density determined by the gravimetric method was systematically higher than the one determined by weight (named geometric density) (Fig. 5). This mismatch was ascribed to the presence of both open and closed pores.

Since the apparent geometric density is affected by the total porosity, while the apparent gravimetric density is affected by pores not accessible by test liquids, air volume fractions corresponding to total and closed porosity were evaluated using Eq. (3). In line with the progressive destructuration of the MFC matrix (Fig. 3) by SiO_2, Fig. 5 shows that the open porosity, calculated as the difference between air volume fractions obtained from geometric and gravimetric apparent densities, progressively increased

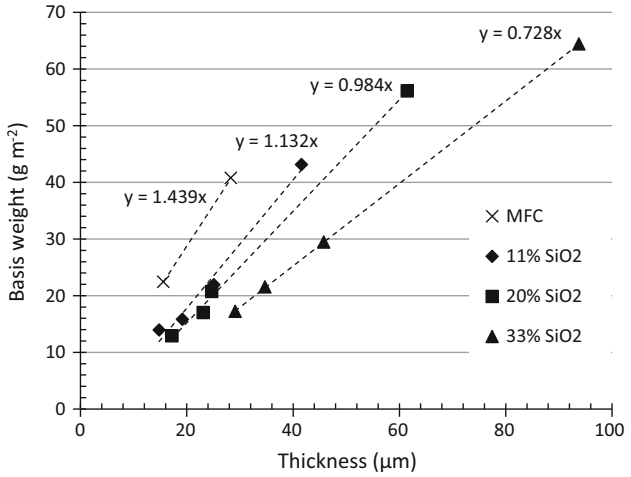

Fig. 4 Basis weight of MFC-SiO_2 nanopaper plotted as a function of sheet thickness and SiO_2 content

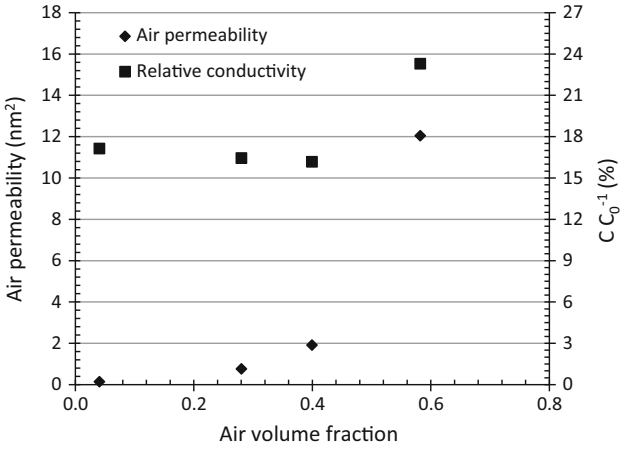

Fig. 6 Intrinsic air permeability and relative Li-ion conductivity along the *Z-axis* of composite sheets plotted as a function of the total air volume fraction

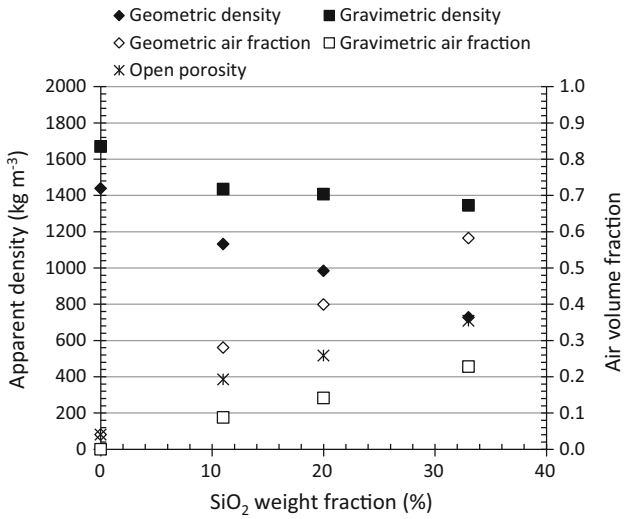

Fig. 5 Influence of the SiO_2 mass fraction on the apparent density and air volume fraction

with the rise of the silica weight fraction. Air permeability and ionic conductivity through the Z-axis of composite films (Fig. 6) exhibited nearly constant values with an abrupt increase for total air volume fractions higher than 0.4 (corresponding to 20 % of SiO_2). As illustrated in Fig. 3, this behaviour was associated to the formation of a percolation path among SiO_2 clusters which favoured air permeation, electrolyte impregnation and Li-ion transport.

Overall, composite sheets displayed air barrier properties which were in line with those obtained for bulk MFC films and coatings [10–13]. Ionic conductivity, which attained 25 % of the bare electrolyte conductivity (corresponding to a Mac Mullin number $N_M = 5$) for the highest SiO_2 mass fraction, was higher than typical numbers of PE–PP based membranes for Li-ion batteries, i.e., 10 % of electrolyte conductivity, $N_M = 10$ [23, 31].

Moreover, the impregnation of a one molar electrolyte, permits to exhibit a conductivity of 1.5 mS cm^{-1} at 25 °C for the highest SiO_2 mass fraction, which is in the range of values needed for a separator.

As observed in a previous study on MFC films [10], tensile properties of composite sheets were strongly affected by the film thickness. Indeed, for all tested SiO_2 mass fractions, the decrease of film thickness was accompanied by a linear decrease of the stress and strain at break (Fig. 7a). Since the Young's modulus was not affected by the sheet thickness (Fig. 7a), this trend was associated to (i) a transition from a slightly plastic to a brittle behaviour and ii) an increased contribution of micron-sized SiO_2 clusters and MFC large debris in fracture nucleation/propagation in thin films.

Stress–strain curves of MFC-SiO_2 sheets with similar thickness of 27 ± 3 µm (Fig. 7b) show that the presence of macroporous SiO_2 clusters impairs the sheet tensile properties. The plot of the Young's modulus and stress at break as a function of the MFC volume fraction (Fig. 8a) highlights a linear decay when ϕ_{MFC} was decreased from 0.96 to 0.33. According to the film microstructure shown in Fig. 3, i.e., macroporous SiO_2 nanoparticle clusters embedded in a dense MFC matrix with limited interphase synergy. The film was described as a bilayer composed by dense MFC and porous SiO_2 clusters. Owing to the porosity of each phase calculated using Eqs. (3)–(5), viz. $\phi_{Air} = 0.04$ and $\phi_{Air} = 0.85$ for the MFC film and SiO_2 clusters, respectively, and the granular nature of the macroporous silica layer, the mechanical resistance was supposed to be provided by the MFC layer.

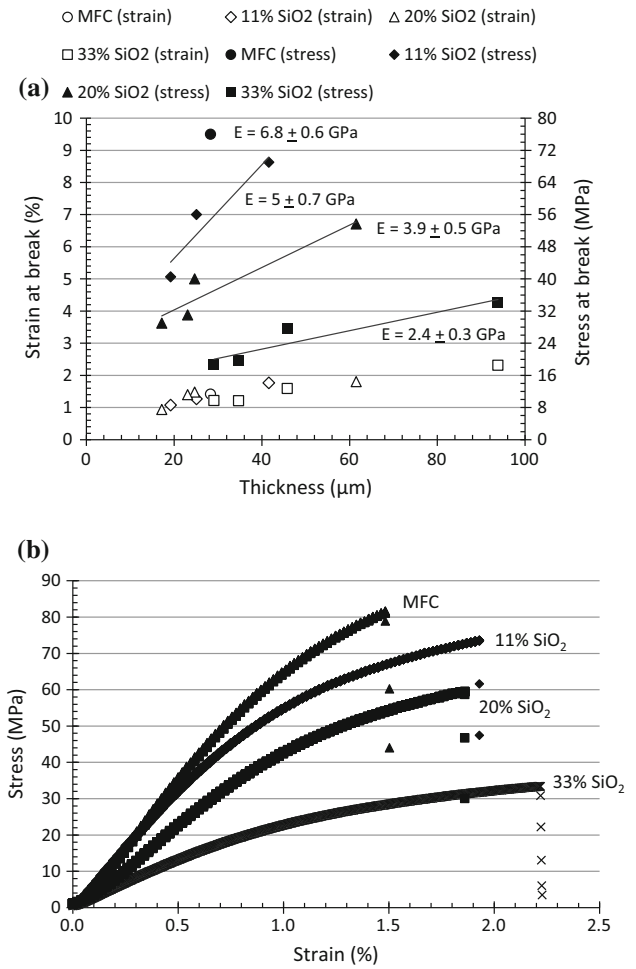

Fig. 7 Tensile properties of composite sheets plotted as a function of film thickness **a** and stress–strain curves of MFC-SiO_2 films with constant thickness of 27 ± 2 μm **b**. Young's moduli (E) given in (**a**) represent the average over all film thickness at constant SiO_2 content

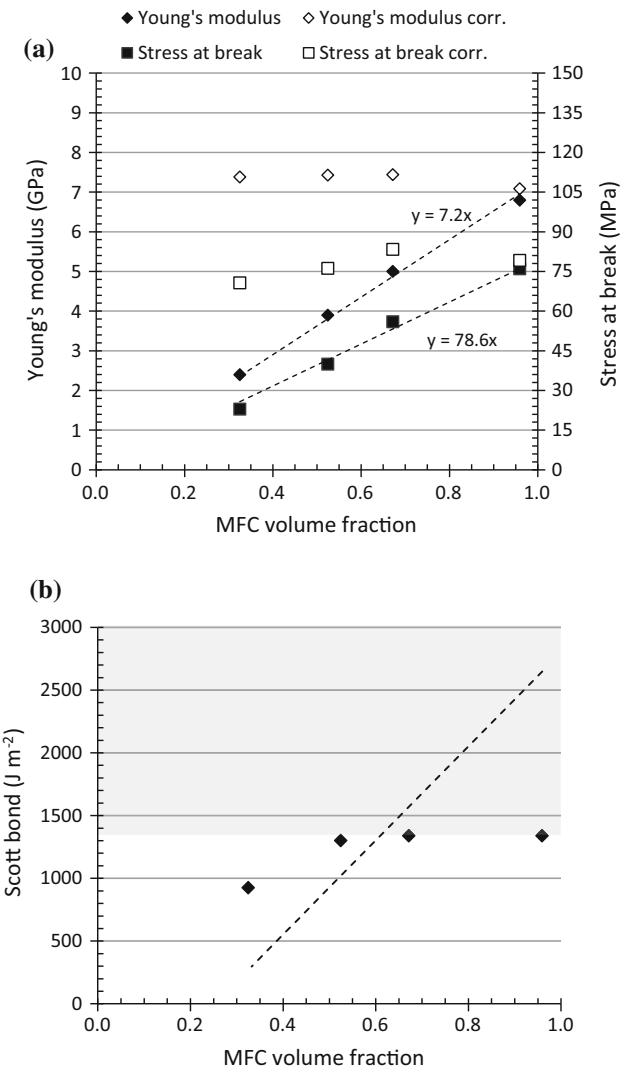

Fig. 8 **a** Effect of the SiO_2 mass fraction on the Young's modulus. *Dotted lines* represent data interpolation with Eqs. (7) and (8). **b** Internal bond strength of composite sheets. The *dotted line* represents the Scott Bond versus cellulose volume fraction correlation for softwood pulp paper [32]. The *grey area* represents the highest bond energy detectable by the testing device

Under these assumptions, the applied stress and the Young's modulus of the MFC layer during traction tests, are given by

$$\sigma_{\mathrm{MFC}} = \frac{\sigma_{\mathrm{App}}}{\phi_{\mathrm{MFC}}}, \tag{7}$$

$$E_{\mathrm{MFC}} = \frac{E_{\mathrm{App}}}{\phi_{\mathrm{MFC}}}, \tag{8}$$

where σ_{App}, E_{App} and ϕ_{MFC} are the apparent stress and Young's modulus and the MFC volume fraction, respectively.

The applied stress and the corresponding Young's modulus of the MFC phase (determined as the slope of straight lines interpolating the experimental data in Fig. 8a) had values close to that obtained for the bulk MFC film (i.e., 78.6 MPa and 7.2 GPa against 75 MPa and 6.8 GPa) and confirmed that the deformation stress was supported by the MFC matrix, while SiO_2 acted as inert macroporous filler.

All composite films exhibited extremely high internal bond strength. Above a MFC volume fraction of 0.67, the Scott Bond was higher than the maximum energy detectable by the testing device (i.e., 1316 J m^{-2}), and even for the lowest MFC volume fraction the internal bond remained higher than that of conventional papers with similar apparent density [32] thus highlighting the excellent bonding ability of MFC.

As summarized in Table 1, when compared to composite MFC-based separators fabricated by filtration, MFC-SiO_2 nanopapers processed by spray deposition display

Table 1 Comparison of composite nanopaper separators fabricated by filtration dewatering

	Fabrication method and composition	Young's modulus (GPa)	Stress at break (MPa)	Strain at break (%)	Mac Mullin number	Intrinsic air permeability (nm^2)	Ionic conductivity in 1 M LiF_6P ($mS\ cm^{-1}$)
This study	*Consist* 2–3 % spray deposition MFC-SiO_2	7–2.4	76–23	1–2.4	6–4	0.7–12	1.5
Ref [24]	*Consist nd* fabric filter CF-SiO_2- Alginate	0.69	45	6.5	4	2000*	2
Ref [22]	*Consist* nd screen filter MFC-Al_2O_3-PVDF	1.3–0.5	30–9	nd	57–6.1	13–190*	0.14–1.28
Ref [23]	*Consist* 0.05–0.6 % copper wire filter time 10 min	*nd*	*nd*	*nd*	5.4–3.1	110–300	1.41–3.15
Ref [31]	*Consist nd* paper filter MFC-isopropyl alcohol	3.2–6.4	21–55	*nd*	9.9–338	*nd*	0.02–0.77

Consist is for slurry consistency and *nd* is for not determined

* Derived from available data

excellent mechanical properties and ionic conductivity thus showing that the fabrication method proposed in this study can represent a viable solution for the rapid production of separators for Li-ion batteries and, overall, of large area composite nanopapers.

Conclusion

Large area MFC-silica composite nanopapers were fabricated by the sequential spray deposition of concentrated MFC-SiO_2 suspensions ad filtration dewatering. Despite the presence of nanoparticles, all suspended solids were retained in the wet MFC mat, and the basis weight of the final composite sheet was tuned from ca. 12 to 65 $g\ m^{-2}$ by varying the deposition conditions (i.e., conveyor speed and suspension concentration).

For a silica mass fraction below 20 %, the structure of composite nanopapers was characterized by the presence of SiO_2 nanoparticle clusters dispersed in a continuous MFC matrix. The low air permeability and constant ionic conductivity measured for SiO_2 mass fractions below 20 % were therefore associated to the presence of closed porosity which did not contribute to air and ion transport.

Above 20 % of SiO_2, percolation paths formed among SiO_2 clusters with a net increase of both air permeability and ionic conductivity which, attaining 1.5 $mS\ cm^{-1}$ in a 1 M $LiPF_6$ electrolyte, was in line with the conductivity of most MFC-based separators for Li-ion batteries and higher than that of conventional PP/PE separators.

Whatever the SiO_2 content, composite nanopapers displayed excellent mechanical properties (i.e. higher than those of conventional paper) with Young's modulus and stress at break ranging from 2.2 to 6.8 GPa and from 23 to 75 MPa when the SiO_2 mass fraction was decreased from 33 to 0 %.

Overall, this work demonstrates that MFC-SiO_2 composite nanopapers and their fabrication by spray deposition are promising alternatives to conventional filtration procedures for the fabrication of composite nanopapers.

Acknowledgements Authors wish to thank the Grenoble Institute of Technology (SEI 2012) and Gravit (Papel project) for supporting this Project. LGP2 is part of the LabEx Tec 21 (Investissements d'Avenir—Grant agreement no ANR-11-LABX-0030) and of the Energies du Futur and PolyNat Carnot Institutes (Investissements d'Avenir—Grant agreements no ANR-11-CARN-007-01 and ANR-11-CARN-030-01).

References

1. Pääkkö M, Ankerfors M, Kosonen H, Nykanen A, Ahola S, Osterberg M, Ruoko-lainen J, Laine J, Larsson PT, Ikkala O, Lindström T (2007) Enzymatic hydrolysis combined with mechanical shearing and high-pressure homogenization for nanoscale cellulose fibrils and strong gels. Biomacromolecules 8:1934–1941
2. Meyer V, Tapin-Lingua S, Da Silva Perez D, Arndt T, Kautto J (2012) Technical opportunities and economic challenges to produce nanofibrillated cellulose in pilot scale: NFC delivery for applications in demonstrations trials. In: Proceed. SUNPAP EU project-final conference, Milan, Italy, 19–20 June 2012. http://sunpap.vtt.fi/finalconference2012.htm
3. Sandquist D (2013) New horizons for microfibrillated cellulose. Appita J 66:156–162
4. Siro I, Plackett D (2010) Microfibrillated cellulose and new nanocomposite materials: a review. Cellulose 17:459–494
5. Siqueira G, Bras J, Dufresne A (2010) Cellulosic bionanocomposites: a review of preparation, properties and applications. Polymers 2:728–765
6. Gonzalez I, Alcala M, Chinga-Carrasco G, Vilaseca F, Boufi S, Mutjé P (2014) From paper to nanopaper: evolution of mechanical and physical properties. Cellulose 21:2599–2609
7. Lavoine N, Desloges I, Dufresne A, Bras J (2012) Microfibrillated cellulose—its barrier properties and applications in cellulosic materials: a review. Carbohydr Polym 90:735–764
8. Zheng G, Cui Y, Karabulut E, Wågberg L, Zhu H, Hu L (2013) Nanostructured paper for flexible energy and electronic devices. MRS Bull 38:320–325

9. Jabbour L, Bongiovanni R, Chauss D, Gerbaldi C, Beneventi D (2013) Cellulose-based Li-ion batteries: a review. Cellulose 20:1523–1545
10. Syverud K, Stenius P (2009) Strength and barrier properties of MFC films. Cellulose 16:75–85
11. Sehaqui H, Liu A, Zhou Q, Berglound LA (2010) Fast preparation procedure for large, flat cellulose and cellulose/inorganic nanopaper structures. Biomacromolecules 11:2195–2198
12. Österberg M, Vartiainen J, Lucenius J, Hippi U, Seppälä J, Serimaa R, Laine J (2013) A fast method to produce strong NFC films as a platform for barrier and functional materials. Appl Mater Interfaces 5:4640–4647
13. Varanasi S, Batchelor WJ (2013) Rapid preparation of cellulose nanofibre sheet. Cellulose 20:211–215
14. Beneventi D, Chaussy D, Zeno E (2014) Rapid nanopaper production by spray deposition of concentrated microfibrillated cellulose slurries. Ind Crops Prod. doi:10.1016/j.indcrop.2014.11.023
15. Beneventi D, Chaussy D, Curtil D, Zolin L, Gerbaldi C, Penazzi N (2014) Highly porous paper loading with microfibrillated cellulose by spray coating on wet substrates. Ind Eng Chem Res 53:10982–10989
16. Beneventi D, Chaussy D, Curtil D, Zolin L, Bruno E, Bongiovanni R, Destro M, Gerbaldi C, Penazzi N, Tapin-Lingua S (2014) Pilot-scale elaboration of graphite/microfibrillated cellulose anodes for Li-ion batteries by spray deposition on a forming paper sheet. Chem Eng J 243:372–379
17. Kulachenko A, Denoyelle T, Galland S, Lindström SB (2012) Elastic properties of cellulose nanopaper. Cellulose 19:793–807
18. Pras O, Beneventi D, Chaussy D, Piette P, Tapin-Lingua S (2013) Use of microfibrillated cellulose and dendritic copper for the elaboration of conductive films from water- and ethanol-based dispersions. J Mater Sci 46:6911–6920
19. Jabbour L, Gerbaldi C, Chaussy D, Zeno E, Bodoardo S, Beneventi D (2010) Microfibrillated cellulose–graphite nanocomposites for highly flexible paper-like Li-ion battery electrodes. J Mater Chem 20:7344–7347
20. Sasso C, Elisa Zeno E, Petit-Conil M, Chaussy D, Belgacem N, Tapin-Lingua S, Beneventi D (2010) Highly conducting polypyrrole/cellulose nanocomposite films with enhanced mechanical properties. Macromol Mater Eng 295:934–941
21. Leijonmarck S, Cornell A, Lindbergh G, Wågberg L (2013) Flexible nano-paper-based positive electrodes for Li-ion batteries-preparation process and properties. Nano Energy 2:794–800
22. Huang X (2014) Performance evaluation of a non-woven lithium ion battery separator prepared through a paper-making process. J Power Source 256:96–101
23. Kim J-H, Kim J-H, Choi E-S, Yu HK, Kim JH, Wu Q, Chun S-J, Lee S-Y, Lee S-Y (2013) Colloidal silica nanoparticle assisted structural control of cellulose nanofiber paper separators for lithium-ion batteries. J Power Source 242:533–540
24. Zhang J, Yue L, Kong Q, Liu Z, Zhou X, Zhang C, Xu Q, Zhang B, Ding G, Qin B, Duan Y, Wang Q, Yao J, Cui G, Chen L (2014) Sustainable, heat resistant and flame-retardant cellulose-based composite separator for high-performance lithium ion battery. Sci Rep 4:3935. doi:10.1038/srep03935
25. Leijonmarck S, Cornell A, Lindbergh G, Wagberg L (2013) Single-paper flexible Li-ion battery cells through a paper-making process based on nano-fibrillated cellulose. J Mater Chem A 1:4671–4677
26. Stana-Kleinschek K, Ribitsch V (1998) Electrokinetic properties of processed cellulose fibers. Colloids Surf A 140:127–138
27. Fall AB, Lindström T, Sundman O, Ödberg L, Wagberg L (2011) Colloidal stability of aqueous nanofibrillated cellulose dispersions. Langmuir 27:11332–11338
28. Maouche-Chergui S, Grohens Y, Balnois E, Lebeau B (2014) Adhesion of silica particles on thin polymer films of flax cell wall. Mater Sci Appl 5:953–965
29. Zhang Y, Chen Y, Westerhoff P, Hristovski K, Crittenden JC (2008) Stability of commercial metal oxide nanoparticles in water. Water Res 42:2204–2212
30. Holmberg M, Wigren R, Erlandsson R, Claesson PM (1997) Interactions between cellulose and colloidal silica in the presence of polyelectrolytes. Colloids Surf A 129–130:175–183
31. Chun S-J, Choi E-S, Lee E-H, Kim JH, Lee S-Y, Lee S-Y (2012) Eco-friendly cellulose nanofiber paper-derived separator membranes featuring tunable nanoporous network channels for lithium-ion batteries. J Mater Chem 22:16618–16626
32. Koubaa A, Koran Z (1995) Measure of the internal bond strength of paper/board. Tappi J 78:103–111